Controlling wideband absorption and electromagnetically induced transparency via a phase change material

ZHENGYONG SONG[a] and BICHUAN ZHANG

Institute of Electromagnetics and Acoustics, Xiamen University - Xiamen 361005, China

Abstract – A terahertz switchable metamaterial is presented with bifunctional properties of absorption and electromagnetically induced transparency based on phase transition of vanadium dioxide. When vanadium dioxide is metal, the designed configuration acts as a wideband absorber consisting of a vanadium dioxide square-shaped array, a dielectric spacer, and a vanadium dioxide continuous film. The working frequency of absorptance larger than 90% ranges from 0.271 THz to 0.592 THz with bandwidth ratio 74.4%. The absorber can work well over a wide range of incident angle for transverse electric polarization and transverse magnetic polarization. When vanadium dioxide is insulator, the designed configuration acts as an analog of electromagnetically induced transparency in the terahertz frequency. The interaction between metallic cross and split ring resonator gives rise to a transparency peak in the transmission spectrum. The performance of electromagnetically induced transparency is robust against polarization and incident angle. This design could provide some prospects in designing switchable terahertz devices, such as the modulator, filter, and optoelectronic components.

Introduction. – In recent years, metamaterials have attracted much research interest due to their multifunctional properties and potential applications, such as perfect lens [1–3], invisible cloak [4–6], and perfect absorber [7–9]. It is an artificially macroscopic composite consisting of structural units smaller than the wavelength. This allows people to characterize their electromagnetic behaviors by effective permittivity and permeability. The metallic or dielectric elements that make up metamaterial can be designed at will to support different responses at any electromagnetic frequency. Their effective permittivity and permeability are not difficult to customize for many different applications from microwave to optical frequencies. So metamaterials provide more opportunities and unprecedented capabilities to control the behaviors of waves. But previous works mostly focus on one function in a single device. At the same time, to change the performance is difficult once the sample is fabricated.

Now, many researches have been devoted to multifunctional materials. Phase change materials are promising candidates for multiband and multifunctional applications

due to their adjustable characteristics. Phase change materials have intriguing properties, such as insulator-metal transition and switchable phenomenon, enabling us to control dielectric permittivity and conductivity under electrical, optical or thermal excitations [10–15]. Vanadium dioxide (VO_2) as one of phase change materials has attracted a lot of attention due to its low phase-transition temperature (340 K) [16–20]. It undergoes a phase transition from a low-temperature monoclinic phase to a high-temperature tetragonal phase. This reversible phase transition occurs on the time scale of some femtoseconds. The conductivity of VO_2 varies by nearly four orders of magnitude under the stimulus of temperature, electric field or light pulse. As a result of this change, many research works have been devoted to VO_2 applications. Several VO_2 tunable devices are reported, such as tunable filter and modulator. In this work, a switchable metamaterial is presented utilizing the phase transition of VO_2. When VO_2 is metal, the designed configuration acts as a wideband absorber. When VO_2 is insulator, the designed configuration acts as an analog of electromagnetically induced transparency in the terahertz frequency.
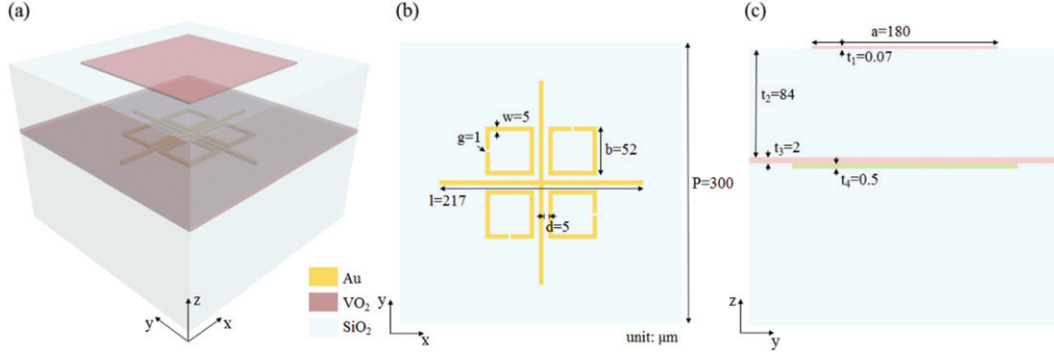
---

[a]E-mail: zhysong@xmu.edu.cn

Fig. 1: (a) Geometrical representation of the designed system. (b) The front view of electromagnetically induced transparency configuration. (c) The side view of the whole system.

Design and method. – Figure 1 illustrates the schematic of the proposed switchable metamaterial. It consists of five layers. Each layer from top to bottom is VO$_2$ square patch, silica (SiO$_2$) spacer, VO$_2$ film, electromagnetically induced transparency structure, and SiO$_2$ substrate. Structural parameters are given as follows: periods in the x and y directions $P = 300\,\mu$m, length of VO$_2$ square patch $a = 180\,\mu$m, length of metallic split ring resonators (SRRs) $b = 52\,\mu$m, length of metallic cross $l = 217\,\mu$m, width of metal $w = 5\,\mu$m, width of air gap in metallic SRRs $g = 1\,\mu$m, distance between metallic SRRs and metallic cross $d = 5\,\mu$m, thickness of VO$_2$ square patch $t_1 = 0.07\,\mu$m, thickness of SiO$_2$ spacer $t_2 = 84\,\mu$m, thickness of VO$_2$ film $t_3 = 2\,\mu$m, thickness of electromagnetically induced transparency structure $t_4 = 0.5\,\mu$m. The frequency-dependent complex dielectric permittivity of VO$_2$ is described by the Drude model $\varepsilon(\omega) = \varepsilon_\infty - \frac{\omega_p^2(\sigma)}{\omega^2 + i\gamma\omega}$ in the terahertz range, where $\varepsilon_\infty = 12$ is the dielectric permittivity in the infinite frequency, $\omega_p(\sigma)$ is the plasma frequency dependent on conductivity and γ is the collision frequency [21–24]. In addition, $\omega_p^2(\sigma)$ and σ are proportional to free carrier density. The plasma frequency at σ can be approximately defined by $\omega_p^2(\sigma) = \frac{\sigma}{\sigma_0}\omega_p^2(\sigma_0)$ with $\sigma_0 = 3 \times 10^5\,$S/m, $\omega_p(\sigma_0) = 1.4 \times 10^{15}\,$rad/s, and $\gamma = 5.75 \times 10^{13}\,$rad/s which is independent of σ. The phase-transition process of VO$_2$ is accompanied by great changes in both conductivity and dielectric permittivity. In the calculation process, different permittivities of VO$_2$ are adopted for different phase states. In our simulation, the conductivity of VO$_2$ is assumed to be $2 \times 10^5\,$S/m (0 S/m) for the metallic (insulating) state. The metal is made of gold with the conductivity of $4.561 \times 10^7\,$S/m, and SiO$_2$ is modeled as a lossless dielectric material with $\varepsilon = 3.8$ [25]. The thickness of SiO$_2$ substrate is considered to be infinite in simulation to avoid Fabry-Pérot resonance. To investigate optical properties of the designed structure, three-dimensional finite element method is used in simulation. Unit cell boundary conditions in the x and y directions are employed to consider periodic arrangement of the structure. The non-uniform
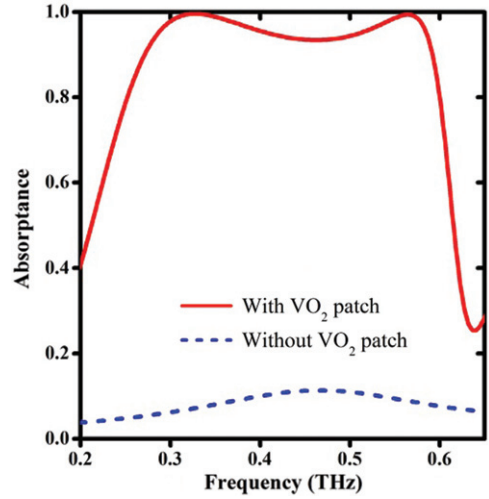

Fig. 2: Absorptance spectra with patch (red solid line) and without patch (blue dashed line) under normal incidence.

mesh is set to reduce the calculating time. A normally incident plane wave is applied along the negative z-direction.

Results and discussions. –

The designed switchable metamaterial acts as a wideband absorber when VO$_2$ is metal. As the thickness of the VO$_2$ film is larger than the skin depth in the terahertz range, incident wave will be prevented and the transmittance (T) of the structure is nearly zero ($T = |S_{21}|^2 \approx 0$). So absorptance (A) is defined as $A = 1 - R - T = 1 - |S_{11}|^2 - |S_{21}|^2 = 1 - R$, where $R = |S_{11}|^2$ represents reflectance. Figure 2 shows the reflectance and absorptance spectra of the designed structure. The red solid line shows that there are two nearly perfect absorption peaks with absorptance >90% in the frequency range of 0.271–0.592 THz under normal incidence. For comparison, the blue dashed line shows absorptance without VO$_2$ squared patch, and it tells the importance of the existence of the VO$_2$ squared patch.
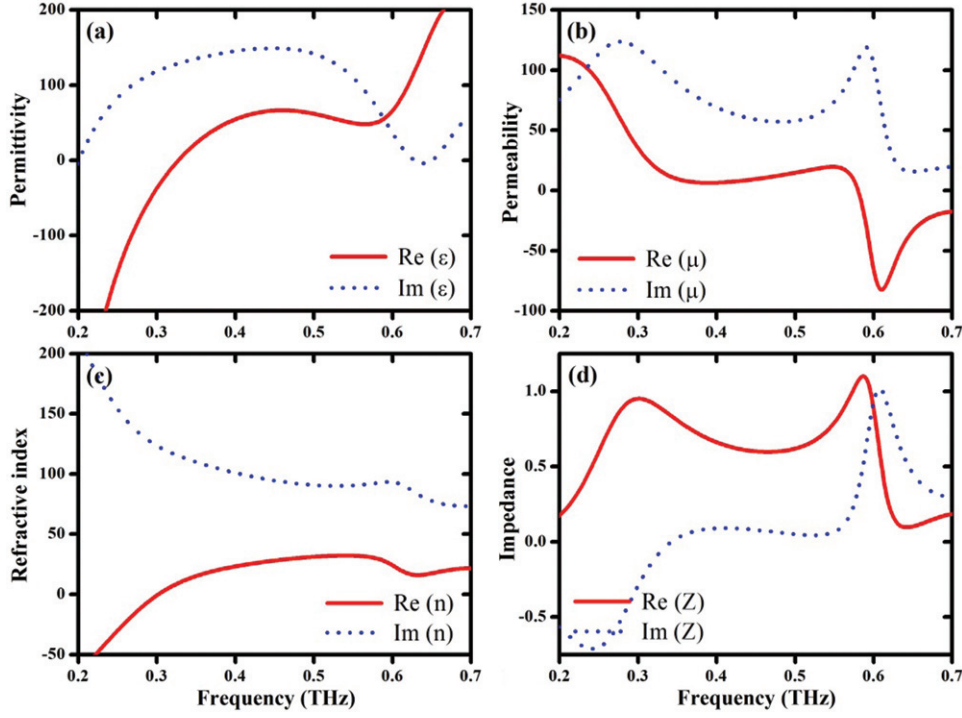
Fig. 3: The retrieved optical parameters: (a) permittivity, (b) permeability, (c) refractive index, and (d) impedance.

In order to obtain ideal absorption, the impedance of the absorber should match that of vacuum. Because the ratio of the central wavelength $695.2\,\mu m$ ($0.432\,THz$) to period $300\,\mu m$ at normal incidence is ~ 2.3, impedance of the designed system can be retrieved by combining the impedance of the square-shaped VO_2 structure and the impedance of dielectric layer and VO_2 bottom plane. Based on the scattering parameter method, effective material parameters (dielectric permittivity ε, magnetic permeability μ, refractive index n, impedance z) can be retrieved by extracting reflection and transmission coefficients (amplitude and phase) for a normally incident wave. Effective impedance is calculated by $Z = \sqrt{\frac{\mu}{\varepsilon}} = \sqrt{\frac{(1+S_{11})^2 - S_{21}^2}{(1-S_{11})^2 - S_{21}^2}}$ under normal incidence [26], and it may be not valid for a large angle of oblique incidence. As is shown in fig. 3(b), two resonances in the effective magnetic response provide the possibility of impedance matching. So the length of the VO_2 squared patch and the thickness of the SiO_2 spacer are the key parameters to control this broadband effect. When dielectric permittivity is equal to magnetic permeability, effective impedance of metamaterial is equal to that of free space. As is shown in fig. 3(d), the real part of effective impedance is close to 1 in two absorption peaks, and the imaginary part is close to zero. Moreover, the imaginary part of the effective refractive index is very large. As a result, there are two matching bands where the reflected wave is minimized.

In the above discussions, the characteristic of this absorber has been studied under normal incidence. It would be better if the design can work well for oblique incidence.
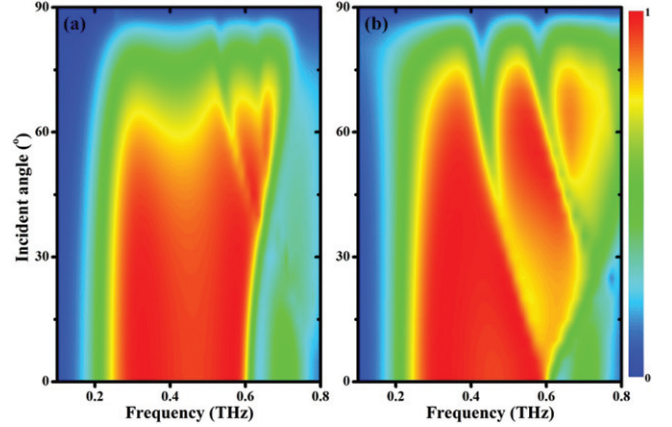

Fig. 4: Absorptance at different incident angles for TE (a) and TM (b) polarizations.

So angular performance deserves to be investigated. The color maps of absorptance as a function of incident angle and frequency are shown in fig. 4. It can be seen that absorptance spectra for transverse electric (TE) and transverse magnetic (TM) polarizations are nearly the same at the very small incident angle. By increasing the incident angle, working bandwidth and intensity for the TE wave in fig. 4(a) are very stable within the incident angle of 40°. When the incident angle is larger than 40°, the performance begins to deteriorate because the intensity of the parallel component of the magnetic field decreases with the increase of incident angle. There are some higher-order
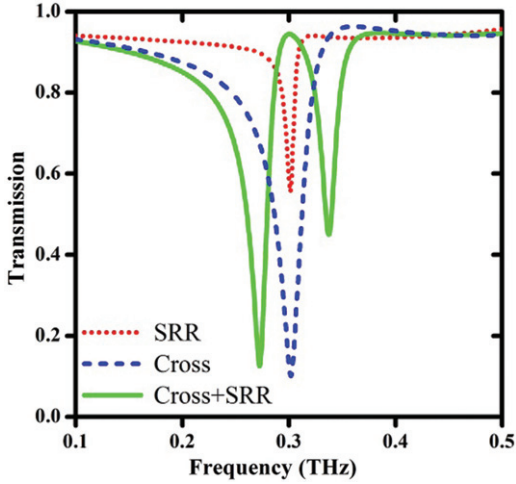
Fig. 5: Simulated transmissions of the isolated metallic cross (blue dashed line), the isolated SRR (red dotted line), and both of them (green line).

Fig. 6: Transmission spectra as a function of frequency and incident angle for TE (a) and TM (b) waves.

modes for the TM wave in fig. 4(b) when the incident angle is larger than 15°.

The designed switchable metamaterial acts as an analog of electromagnetically induced transparency when VO_2 is insulator. Electromagnetically induced transparency is the result of quantum destructive interference in a three-level atomic system. It generates a transparent window in an opaque spectrum. But the requirements of high-intensity laser and low-temperature environment strongly hinder the development of electromagnetically induced transparency in many applications. Recently, lots of efforts have been done to mimic the behavior of electromagnetically induced transparency. In plasmonic metamaterials, near-field coupling between bright mode and dark mode can generate a transparent window.

In order to investigate the analog of electromagnetically induced transparency in the designed metamaterial, the isolated metallic cross, the isolated SRR, and both of them are simulated. The corresponding transmission spectra are shown in fig. 5. The metallic cross exhibits a typical localized plasmonic resonance at 0.302 THz, and it is the direct response to incident wave. This resonance has a broad line width. SRR can also support a resonance with a narrow line width at 0.301 THz. These two resonances almost have the same resonant frequency. When two types of resonators are arranged within a unit cell, a transparency peak is clearly observed at 0.30 THz with an amplitude of 94.4% between two resonant dips around 0.272 THz and 0.337 THz. Near-field coupling between metallic cross and metallic SRR leads to destructive interferences and gives rise to an analog of electromagnetically induced transparency.

The influences of incident angle on electromagnetically induced transparency are studied. In order to investigate the angular dependence of the metamaterial, figs. 6(a), (b)
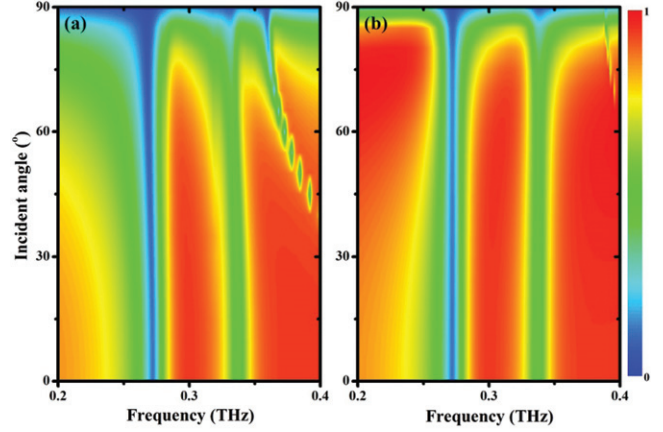
show the simulated transmission spectra as a function of incident angle and frequency. When the incident angle is smaller than 45°, the transmission properties of the metamaterial are independent of the incident angle for TE and TM waves. For the TE wave, with the increase of incident angle, bandwidth of transmission peak narrows and intensity weakens. This is because the vertical component of the magnetic field of the TE wave increases with the increase of incident angle. When the incident angle is larger than 45°, the transmission intensity of the TM wave changes little and the bandwidth of the transmission peak broadens a little with the increase of incident angle. This is because the vertical component of the electric field of TM wave increases with the increase of incident angle.

Conclusion. – To summarize, a multilayer metamaterial is designed with switchable properties of absorption and electromagnetic induced transparency. When VO_2 is metal, it acts as a wideband absorber consisting of VO_2 patches, a dielectric spacer, and a VO_2 film. The simulated results show that absorptance larger than 90% is in the frequency of 0.271–0.592 THz. The performance of absorption is robust against the incident angle. When VO_2 is insulator, the designed configuration acts as an analog of electromagnetic induced transparency in the terahertz frequency. The interaction between metallic cross and SRRs gives rise to a pronounced transparency window in the transmission spectrum. The performance of electromagnetic induced transparency is insensitive to incident angle. This work could have many fascinating prospects on switchable meta-devices [27–30], such as terahertz active filter, modulator, and delay component.

<center>∗ ∗ ∗</center>

data analysis, and modified the manuscript. ZS conceived the idea, wrote the paper, and supervised the whole work. All authors read and approved the final manuscript. The authors declare that they have no competing interests.

REFERENCES

[1] Pendry J. B., *Phys. Rev. Lett.*, **85** (2000) 3966.
[2] Fang N., Lee H., Sun C. and Zhang X., *Science*, **308** (2005) 534.
[3] Ono A., Kato J. and Kawata S., *Phys. Rev. Lett.*, **95** (2005) 267407.
[4] Pendry J. B., Schurig D. and Smith D. R., *Science*, **312** (2006) 1780.
[5] Ergin T., Stenger N., Brenner P., Pendry J. B. and Wegener M., *Science*, **328** (2010) 337.
[6] Li J. and Pendry J. B., *Phys. Rev. Lett.*, **101** (2008) 203901.
[7] Landy N. I., Sajuyigbe S., Mock J. J., Smith D. R. and Padilla W. J., *Phys. Rev. Lett.*, **100** (2008) 207402.
[8] Hao J. M., Wang J., Liu X. L., Padilla W. J., Zhou L. and Qiu M., *Appl. Phys. Lett.*, **96** (2010) 251104.
[9] Song Z., Wang Z. and Wei M., *Mater. Lett.*, **234** (2019) 138.
[10] Shportko K., Kremers S., Woda M., Lencer D., Robertson J. and Wuttig M., *Nat. Mater.*, **7** (2008) 653.
[11] Chen Y. G., Kao T. S., Ng B., Li X., Luo X. G., Lukyanchuk B., Maier S. A. and Hong M. H., *Opt. Express*, **21** (2013) 13691.
[12] Wei M., Song Z., Deng Y., Liu Y. and Chen Q., *Mater. Lett.*, **236** (2019) 350.
[13] Hira T., Homma T., Uchiyama T., Kuwamura K., Kihara Y. and Saiki T., *Appl. Phys. Lett.*, **106** (2015) 031105.
[14] Yoo S., Gwon T., Eom T., Kim S. and Hwang C. S., *ACS Photon.*, **3** (2016) 1265.
[15] Yin X. H., Steinle T., Huang L. L., Taubner T., Wuttig M., Zentgraf T. and Giessen H., *Light-Sci. Appl.*, **6** (2017) e17016.
[16] Dicken M. J., Aydin K., Pryce I. M., Sweatlock L. A., Boyd E. M., Walavalkar S., Ma J. and Atwater H. A., *Opt. Express*, **17** (2009) 18330.
[17] Kats M. A., Sharma D., Lin J., Genevet P., Blanchard R., Yang Z., Qazilbash M. M., Basov D. N., Ramanathan S. and Capasso F., *Appl. Phys. Lett.*, **101** (2012) 221101.
[18] Liu L., Kang L., Mayer T. S. and Werner D. H., *Nat. Commun.*, **7** (2016) 13236.
[19] Song Z., Chen A. and Zhang J., *Opt. Express*, **28** (2020) 2037.
[20] Cai H., Chen S., Zou C., Huang Q., Liu Y., Hu X., Fu Z., Zhao Y., He H. and Lu Y., *Adv. Opt. Mater.*, **6** (2018) 1800257.
[21] Liu M., Hwang H. Y., Tao H., Strikwerda A. C., Fan K., Keiser G. R., Sternbach A. J., West K. G., Kittiwatanakul S., Lu J., Wolf S. A., Omenetto F. G., Zhang X., Nelson K. A. and Averitt R. D., *Nature*, **487** (2012) 345.
[22] Chu Q., Song Z. and Liu Q. H., *Appl. Phys. Express*, **11** (2018) 082203.
[23] Wang S., Kang L. and Werner D. H., *Sci. Rep.*, **7** (2017) 4326.
[24] Song Z., Deng Y., Zhou Y. and Liu Z., *Opt. Express*, **27** (2019) 5792.
[25] Naftaly M. and Miles R. E., *J. Appl. Phys.*, **102** (2007) 043517.
[26] Smith D. R., Schultz S., Markos P. and Soukoulis C. M., *Phys. Rev. B*, **65** (2002) 195104.
[27] Liu N., Mesch M., Weiss T., Hentschel M. and Giessen H., *Nano Lett.*, **10** (2010) 2342.
[28] Mou N., Sun S., Dong H., Dong S., He Q., Zhou L. and Zhang L., *Opt. Express*, **26** (2018) 11728.
[29] Sun S., He Q., Hao J., Xiao S. and Zhou L., *Adv. Opt. Photon.*, **11** (2019) 380.
[30] Mou N., Liu X., Wei T., Dong H., He Q., Zhou L., Zhang Y., Zhang L. and Sun S., *Nanoscale*, **12** (2020) 5374.